nature neuroscience

Adaptation of the simple or complex nature of V1 receptive fields to visual statistics

Julien Fournier[1], Cyril Monier[1], Marc Pananceau[1,2] & Yves Frégnac[1]

Receptive fields in primary visual cortex (V1) are categorized as simple or complex, depending on their spatial selectivity to stimulus contrast polarity. We studied the dependence of this classification on visual context by comparing, in the same cell, the synaptic responses to three classical receptive field mapping protocols: sparse noise, ternary dense noise and flashed Gabor noise. Intracellular recordings revealed that the relative weights of simple-like and complex-like receptive field components were scaled so as to make the same receptive field more simple-like with dense noise stimulation and more complex-like with sparse or Gabor noise stimulations. However, once these context-dependent receptive fields were convolved with the corresponding stimulus, the balance between simple-like and complex-like contributions to the synaptic responses appeared to be invariant across input statistics. This normalization of the linear/nonlinear input ratio suggests a previously unknown form of homeostatic control of V1 functional properties, optimizing the network nonlinearities to the statistical structure of the visual input.

The distinction between simple and complex cells[1] relies on the degree of spatial segregation and linearity of responses to contrasts of opposite signs. Simple receptive fields are classically considered to be linear feature detectors, computing a weighted sum of the local contrast of the image[1–4], whereas complex receptive fields exhibit nonlinear spatial summation properties, resulting in response invariance with regard to position or contrast polarity[1,5–7].

Most extracellular surveys have reported V1 receptive fields with intermediate behaviors[2,6,8], and intracellular recordings have shown that the separation between simple and complex cells hides a continuous distribution of synaptic inputs with regard to their degree of linearity[9]. In spite of the general acceptance that simple and complex cells correspond to distinct balance levels between linear and nonlinear contributions at the synaptic level[10–12], few studies have investigated whether the functional expression of the simple or complex nature of V1 receptive fields depends, in the same cell, on the spatiotemporal statistics of the stimulus[13,14]. This may be surprising, as gain control mechanisms are known to ensure the contrast invariance of the cell selectivity[15,16], and it is well established that adaptation to stimulus contrast does not have the same effect on the simple-like and complex-like components of V1 cell responses when assessed with drifting gratings[17,18]. Still, most studies of receptive field adaptation to visual statistics have focused either on linear receptive field components in simple cells or on nonlinear components in complex cells[19–23], and not on the differential adaptation of these two receptive field components in the same receptive field.

We addressed this question by estimating synaptic and discharge fields of cat V1 cells recorded intracellularly in three white-noise stimulus conditions: sparse noise, ternary dense noise and Gabor noise. We found that the relative weights of the simple-like and complex-like components of the same receptive field adapted to the spatiotemporal statistics of the stimulus such that the respective contributions of these two functional components in the synaptic response remained in constant proportion across stimulus conditions once the receptive field was convolved with the visual stimulation sequence. This adaptation was not a straightforward scaling of the amplitudes of these receptive field components, but instead resulted from differential changes in both their spatial extents and their temporal dynamics. These findings suggest that the functional properties of the V1 network, as measured from V1 receptive field estimates, are not fixed, but instead adapt to the statistical properties of the visual input.

RESULTS

We recorded 32 neurons intracellularly in cat area 17 and mapped their receptive fields with three protocols: sparse noise, ternary dense noise and Gabor noise (**Fig. 1a**). Comparison across stimulus conditions was conducted at the subthreshold synaptic integration level and at the spiking output level. We first focused our analysis on receptive field estimates obtained in the spatiotemporal domain (sparse noise and dense noise) and further extended the comparison to receptive fields estimated in the orientation domain (Gabor noise).

Stimulus dependence of V1 receptive field estimates

Most previous receptive field studies using ternary white-noise stimuli decomposed the cell input-output relationship into elementary responses to bright and dark stimuli[1,6,9,24], namely ON and OFF subfields, respectively. In this framework, the simple or complex nature of the receptive field was defined with different types of indexes measuring the degree of spatial segregation or antagonism between ON and OFF spatial profiles[24]. In studies using drifting gratings, simple and complex behaviors were quantified according to the degree

[1]Unité de Neuroscience, Information et Complexité (CNRS-UNIC), UPR CNRS 3293, Gif-sur-Yvette, France. [2]Université Paris-Sud, Orsay, France. Correspondence should be addressed to J.F. (Fournier@unic.cnrs-gif.fr) or Y.F. (fregnac@unic.cnrs-gif.fr).

Received 21 March; accepted 10 May; published online 17 July 2011; doi:10.1038/nn.2861

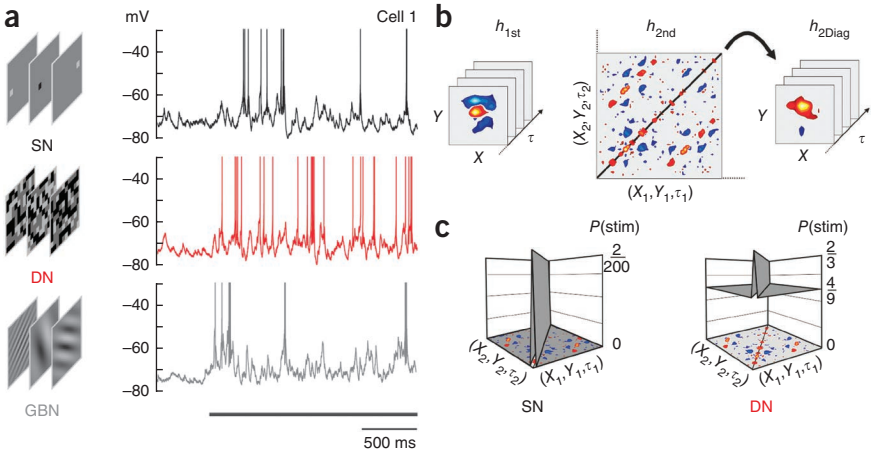

Figure 1 White-noise stimuli and second-order Volterra receptive field decomposition. (**a**) Example of single-trial intracellular responses evoked in the same cell (cell 1) by sparse (SN, black), dense (DN, red) and Gabor noise (GBN, gray) stimuli. The visual stimulation period is indicated by the horizontal black line. Spike amplitudes have been cut off at –30 mV to facilitate the comparison between V_m fluctuation dynamics. (**b**) First- and second-order Volterra kernels were estimated using a least-squares method. In this decomposition, the h_{1st} kernel linearly filters the stimulus contrast variations and can be considered to be the simple-like part of the receptive field in the strict sense. In contrast, the second-order diagonal h_{2Diag} corresponds to the projection of the second-order receptive field nonlinearities in the first-order stimulus space, pooling receptive field components independent of the contrast sign, and can be considered as the complex-like part of the receptive field. The feature selectivity underlying this h_{2Diag} complex-like component is provided by the off-diagonal terms of the second-order kernel h_{2nd}. (**c**) Probability of stimulation (P(stim)) of the second-order kernel by sparse noise (left, 10 × 10 stimulation grid) and dense noise (right). In contrast with dense noise stimuli, pixels are activated one at a time in sparse noise condition. Consequently, off-diagonal components of the second-order kernel are barely stimulated by sparse noise compared to the diagonal elements, making their estimation irrelevant in sparse stimulation contexts.

of linearity of the cell response with respect to the spatial phase of the stimulus at the preferred orientation and spatial frequency[2,5,6,8]. Here, we attempted to reconcile both classifications by switching from the classical ON~OFF decomposition of white-noise receptive field estimates to a Volterra receptive field expansion into first- (h_{1st}) and second-order (h_{2nd}) kernels (**Fig. 1b**). In this decomposition, the filter h_{1st} represents the part of the receptive field that responds linearly with contrast polarity, whereas the second-order diagonal (h_{2Diag}) pools nonlinear receptive field components independent of the contrast sign. The selectivity of this h_{2Diag} component to stimulus features such as orientation and spatial frequency is defined by the off-diagonal elements of the second-order kernel[5].

Because of the high dimensionality of this second-order kernel, we estimated off-diagonal interaction terms only in the dense noise condition for subthreshold responses. On the one hand, the number of collected spikes was generally too small to proceed to a complete estimate of the spiking second-order kernel. On the other hand, off-diagonal components were barely stimulated with sparse noise, making their estimation irrelevant in this stimulation context (**Fig. 1c**). Although this limitation restricted the comparison of receptive field estimates to the h_{1st} and h_{2Diag} filters, it was not critical with regard to our study; the estimation of the apparent simple or complex nature of the receptive field can be directly assessed from the balance between these two kernels without any knowledge of the feature selectivity underlying the complex-like component h_{2Diag}. This truncated second-order Volterra expansion is computationally equivalent to the ON~OFF decomposition; h_{1st} and h_{2Diag} kernels are strictly related to the difference and the sum, respectively, between ON and OFF kernels[7]. However, representing V1 receptive fields as h_{1st} and h_{2Diag} components makes it easier to distinguish along both spatial and temporal receptive field dimensions between the net linear push-pull contribution (the simple-like receptive field component in the strict sense) and the nonlinear contribution that responds in the same way to both contrast polarities (the complex-like receptive field component).

The Volterra decomposition of two representative cells are shown in **Figure 2**. Whether we considered the synaptic or the spiking receptive field estimates, the comparison between sparse and dense visual contexts revealed the same effect. The h_{1st} and h_{2Diag} waveforms were both substantially reduced in amplitude when switching from sparse to dense noise (**Fig. 2b**,**d**), and they also exhibited systematic changes in their respective spatiotemporal organizations (**Fig. 2a**,**c**). In the sparse noise condition, the receptive field of cell 1 expressed a weak simple-like component and a relatively large complex-like contribution, whereas dense noise stimulation of the same cell enhanced the simple-like contribution and reshaped the complex-like component by shrinking its spatial and temporal extent. Similarly, in cell 2, the receptive field switched from balanced simple-like and complex-like components in the sparse noise condition to an almost complete suppression of the complex-like contribution with dense noise. The same stimulus-dependent changes were observed in all of the cells that we recorded; whatever the degree of linearity of the receptive field estimated in the sparse context, the balance between simple-like and complex-like receptive field components was modified so to express stronger linear/simple-like components (h_{1st}) relative to the nonlinear/complex-like components (h_{2Diag}) in the dense context (see also **Supplementary Fig. 1**). In the classical ON~OFF perspective, the comparison of receptive field estimates between sparse and dense noise conditions led to the same conclusion: ON and OFF subfields exhibited much smaller overlap and/or stronger antagonism in the dense than in the sparse visual context (**Supplementary Fig. 2**).

Receptive field simpleness and gain controls

To quantify the balance between simple-like and complex-like receptive field components in each stimulus condition, we defined a simpleness index (SI) that measures the spatiotemporal energy of the linear h_{1st} kernel relative to the sum of the h_{1st} and h_{2Diag} spatiotemporal energies (see Online Methods). The SI thus tends to 0 for complex receptive fields and converges to 1 for simple receptive fields. Dense noise stimuli resulted in a significant increase of receptive field simpleness compared with sparse noise, both at the subthreshold and spiking levels ($P << 0.001$, paired Student's t test; **Fig. 3a**,**b**). If we applied the $SI = 0.5$ threshold as a distinction criterion, the synaptic receptive fields could be classified as simple in 81% of cases in the dense noise context versus only 28% in the sparse noise condition. A similar switch in receptive field type was found at the spiking level with 75% of simple cells with dense noise versus 33% with sparse noise.

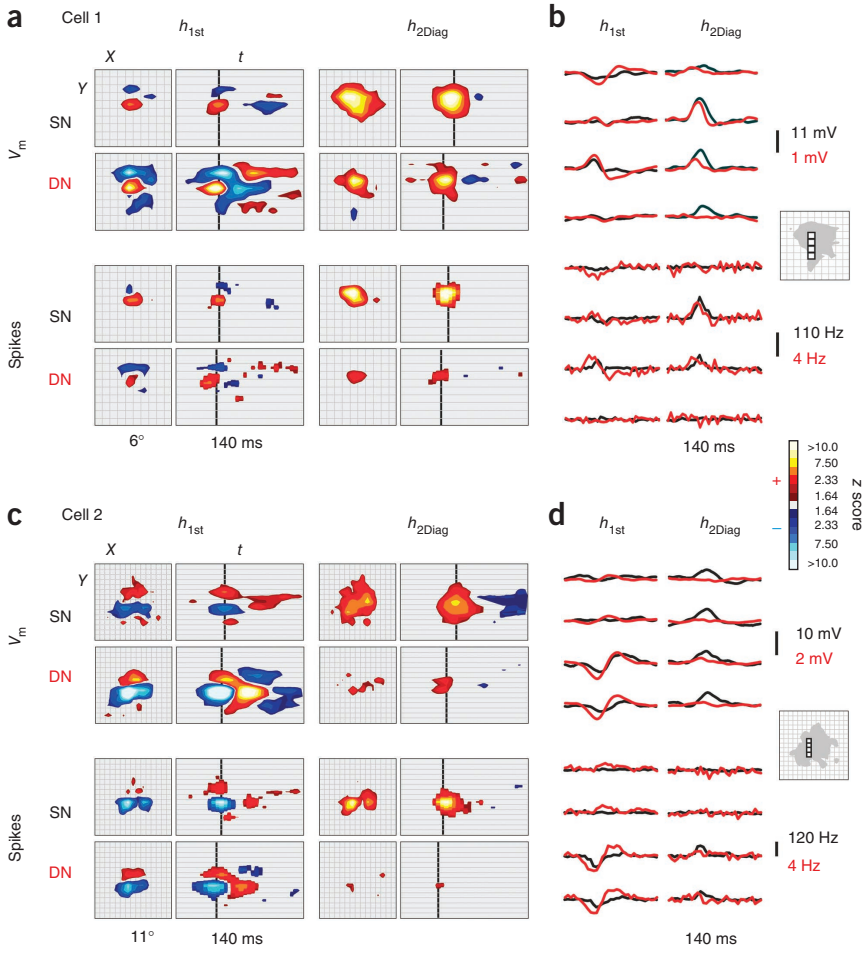

Figure 2 Stimulus dependence of simple-like and complex-like receptive field components. (**a**) First-order kernel (left column, simple-like, h_{1st}) and second-order diagonal kernel (right column, complex-like, h_{2Diag}) of subthreshold (V_m) and spiking (spikes) receptive field estimates for a typical V1 cell (cell 1). Kernels are depicted as spatial (*X*, *Y*) and two-dimensional spatiotemporal (*Y*, time (*t*)) *z*-scored maps. The *X*,*Y* spatial maps are shown for the lag time corresponding to their maximal spatial extent (indicated by the vertical black line in *Y*,*t* spatiotemporal profiles). The thin gray lines show the pixel size used for sparse and dense noise. (**b**) Examples of elementary responses corresponding to positions indicated in the inset, overlaid over the shaded responsive area. Note the differences of scale between sparse (black) and dense noise (red) waveforms, reflecting a divisive gain control of both simple-like and complex-like receptive field components when switching from sparse to dense visual stimulation. (**c**,**d**) Data are presented as in **a**,**b** for another example cell (cell 2).

The difference in *SI* trends observed between sparse and dense noise conditions when comparing spike- and membrane potential (V_m) measures did not result from a change in the spike threshold nonlinearity, but rather from the effect of the half rectification of the V_m response on the read-out of the receptive field simpleness (**Supplementary Fig. 3**).

We found that a markedly uniform behavior emerged from the various recorded cells when comparing the *SI* values computed for dense and sparse conditions: all of the data points, each representing one cell, were positioned along a continuous smooth curve in the bivariate correlation plot between dense and sparse noise *SI* values (**Fig. 3a**,**b**). We quantified the change in gain of the h_{1st} and h_{2Diag} receptive field components by a gain factor ($gain_{SN/DN}$), defined as the ratio of the Euclidian norms of the kernel estimates when switching from sparse to dense noise. Over the population, the $gain_{SN/DN}$ values measured on first-order synaptic components were consistent, on average, with an optimal gain control that would normalize the linear filter output relative to the eightfold difference between the s.d. of luminance values in sparse and dense noise conditions (mean h_{1st} $gain_{SN/DN}$ = 7.75 at the subthreshold level; **Fig. 3c**). For the complex-like receptive field component h_{2Diag}, the $gain_{SN/DN}$ values were all larger than for simple-like components, both at the synaptic and spiking

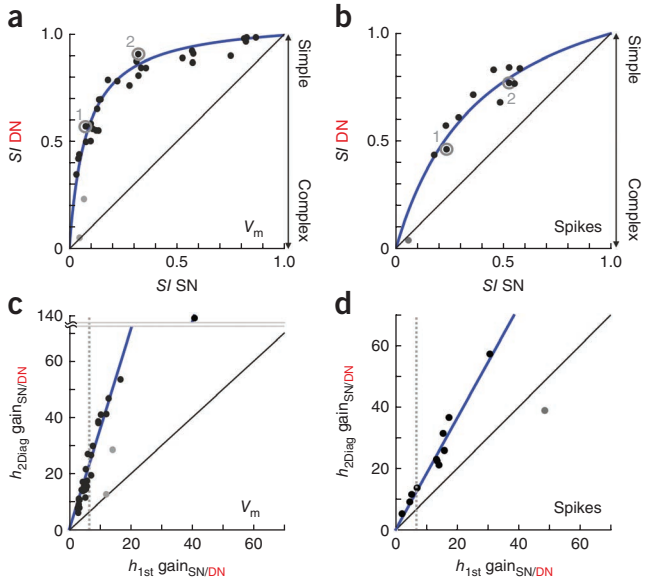

Figure 3 Receptive field Simpleness and gain control of simple-like and complex-like receptive field components. (**a**,**b**) Comparison over the population of recorded cells of the *SI* measured from synaptic (**a**) or spiking (**b**) receptive field estimates between sparse and dense noise conditions. All points lie above the identity line, indicating that all receptive fields underwent a systematic change in the balance between simple-like and complex-like receptive field components such that they appeared to be more simple in dense than in sparse noise conditions. The data points corresponding to the example cells (shown in **Fig. 2**) have been circled. (**c**,**d**) Comparison between the $gain_{SN/DN}$ measured for complex-like (h_{2Diag} $gain_{SN/DN}$) and simple-like (h_{1st} $gain_{SN/DN}$) receptive field components, at the subthreshold (**c**) and spiking (**d**) levels. The gain factors affecting the complex-like components were systematically higher and appeared to be linearly related to the amplitude of the gain controls measured from the first-order component h_{1st}, except for two outliers (gray symbols) (blue regression lines; V_m: slope = +3.53, r^2 = 0.98, $P << 0.01$, n = 30; spikes: slope = +1.81, r^2 = 0.90, $P << 0.01$, n = 11). The vertical dotted line indicates the value that we would expect from perfectly adapting linear receptive field components; h_{1st} $gain_{SN/DN}$ would correspond to the ratio of sparse and dense noise s.d. of luminance values (~8.16, see Online Methods).

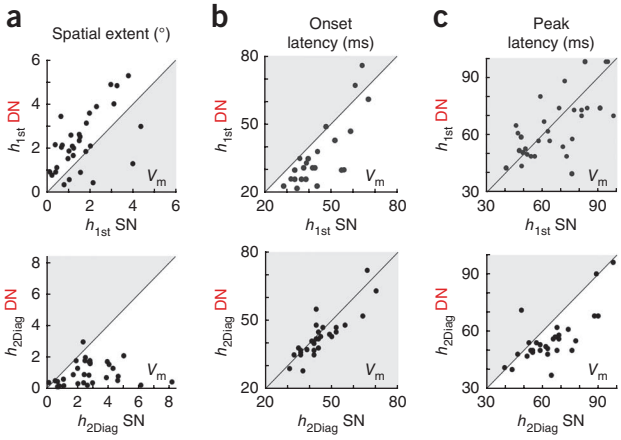

Figure 4 Spatiotemporal reconfiguration of simple-like and complex-like receptive field components. (**a**) Comparison between dense noise and sparse noise conditions of the maximal spatial extents of significant responses measured in simple-like (h_{1st}, top) and complex-like (h_{2Diag}, bottom) receptive field components (units, visual degree of apparent diameter). Although simple-like receptive field components appeared to be significantly larger in the dense noise than in the sparse noise condition (paired Student's *t* test, $P < 0.01$), the complex-like receptive field components were significantly smaller (paired Student's *t* test, $P << 0.01$). (**b**) Comparison of onset latencies of simple-like (h_{1st}, top) or complex-like (h_{2Diag}, bottom) receptive field components between dense noise and sparse noise conditions. (**c**) Comparison of peak latencies of simple-like (h_{1st}, top) or complex-like (h_{2Diag}, bottom) receptive field components between dense noise and sparse noise conditions.

levels (mean h_{2Diag} $gain_{SN/DN}$ = 25.0 at the subthreshold level, $P << 0.001$, paired Student's *t* test; **Fig. 3c**), consistent with an increased linearity of the receptive fields in the dense noise context.

Notably, despite the large variability in h_{1st} $gain_{SN/DN}$, the gain controls affecting the complex-like (h_{2Diag} $gain_{SN/DN} = \beta$) and simple-like (h_{1st} $gain_{SN/DN} = \alpha$) receptive field synaptic components were related to each other according to a linear relationship over the cell population (slope $k = \beta/\alpha = 3.53$, $r^2 = 0.98$, $P < <0.01$, $n = 30$; **Fig. 3c**). A similar linear relationship was also observed at the spiking level, with a half slope value (slope $k = \beta/\alpha = 1.81$, 11 of 12, $r^2 = 0.90$, $n = 11$; **Fig. 3d**). This proportionality rule explains the smoothness of the global behavior observed in the *SI* (**Fig. 3a**,**b**, see Online Methods) and the best fit at the population level is given by a hyperbolic function parameterized by the slope of the regression (see **Supplementary Note 1**).

$$SI_{DN} = \frac{SI_{SN}}{SI_{SN} + \left(\frac{\alpha}{\beta}\right)^2 \times (1 - SI_{SN})}$$

For all cells, h_{1st} and h_{2Diag} $gain_{SN/DN}$ values were larger than 1, reflecting a systematic downscaling of the full receptive field from sparse to dense noise conditions (**Supplementary Fig. 4**). They also appeared to be negatively correlated with the *SI* values, indicating that the more simple the cell, the weaker the gain controls on simple-like and complex-like receptive field components when switching from sparse to dense noise (**Supplementary Fig. 5**).

As illustrated by cell 1 and cell 2 (**Fig. 2**), these gain controls are not a straightforward rescaling of the kernel profiles, but instead imply differential changes, at a synaptic level, in both their apparent spatial extent and their temporal dynamics across stimulus conditions. Spatially, the visuotopic extents of first-order receptive field components were enlarged when switching from sparse to dense noise (**Fig. 4a**), whereas second-order diagonal subfields shrunk conversely (**Fig. 4a**). Temporally, first-order receptive field components (h_{1st}) had a shorter latency in the dense noise than in the sparse noise condition (**Fig. 4b**), whereas the second-order receptive field components (h_{2Diag}) did not change in latency (**Fig. 4b**), but were reduced in duration (**Fig. 4c**). This late shortening suggests that delayed inhibition might reduce the propagation of nonlinear/complex-like components in the dense noise regime and restrict their response integration time relative to the sparse noise condition. The functional importance of these receptive field changes was confirmed by the ability of subthreshold receptive fields to predict responses to new sequences of sparse and dense noise stimuli (validation set of single trial data, see Online Methods); even though, at the population level, sparse noise and dense noise receptive fields only partially predicted responses corresponding to the same stimulus condition, they almost systematically failed to explain the response to the other stimulus class as well as the receptive field estimated in the same stimulus condition as the validation dataset ($P < <0.01$, paired Student's *t* test; **Supplementary Fig. 6**).

V1 receptive field simpleness adapts to visual statistics

To measure the balance between simple-like and complex-like synaptic contributions once the receptive field is convolved with the stimulus, we computed another simpleness index (*SI**), based on the reconstructed outputs of the first- and second-order kernel estimates (**Fig. 5a** and Online Methods). This convolution resulted in a realignment of the *SI* values; over the cell population, the *SI** values were indistinguishable between sparse and dense noise conditions (**Fig. 5b**), suggesting that the balance between simple-like and complex-like contributions remains unchanged in V1 cell synaptic activity whether the visual test noise is sparse or dense.

To test a possible generalization to other visual input statistics, we measured the simple or complex nature of synaptic and spiking receptive fields estimated with Gabor noise stimuli (for 20 of 32 cells; **Supplementary Fig. 7**). The *SI* computed in the Gabor noise condition revealed that synaptic (**Fig. 5c**) and spiking receptive fields (**Supplementary Fig. 7c**) were far more complex with Gabor noise than with dense noise (or, to a lesser extent, with sparse noise; data not shown). This result is consistent with our previous finding, as, for cortical cells, the Gabor noise protocol can be considered to be a sparse stimulation in the Fourier domain. Accordingly, we found that no difference was noticeable between *SI** values measured in the Gabor noise and the dense (**Fig. 5c**) or the sparse noise (data not shown) conditions, which reinforces and generalizes our hypothesis of a normalization of the simpleness of the visually evoked synaptic drive.

This realignment of the *SI* values observed after convolving the receptive fields with the different stimulus sequences was visible even when considering only the h_{2Diag} filter for reconstructing the complex-like component of the dense noise response (**Supplementary Fig. 8**). Thus, this normalization cannot simply be explained by the recruitment of the off-diagonal terms of the second-order kernel in the dense noise context; the stimulus-dependent changes observed on the second-order diagonal h_{2Diag} contribute substantially to the invariance of the simpleness of the reconstructed receptive field outputs across input statistics.

The most sophisticated fits of V1 receptive fields in previous studies relied on a convergence of multiple parallel linear subunits whose outputs were combined nonlinearly[12]. In this model architecture, the afferent filters can be considered as simple-like or complex-like

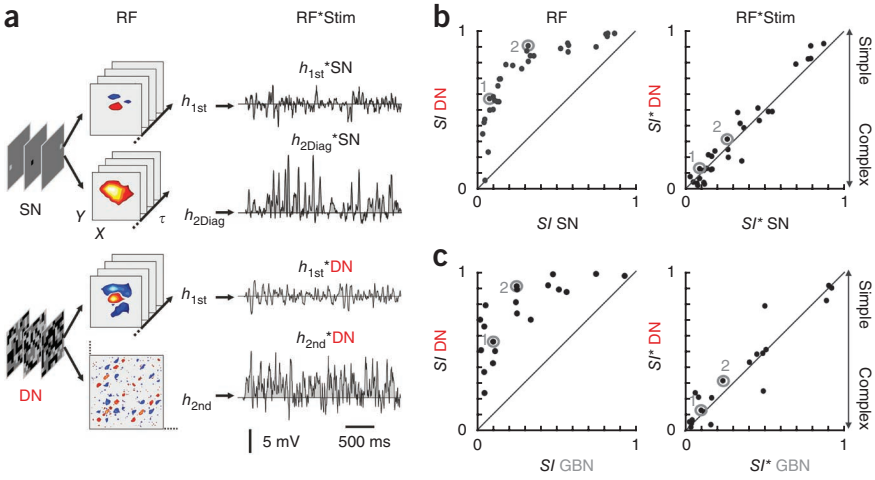

Figure 5 V1 receptive field simpleness adapts to visual statistics. (**a**) In each stimulus condition, the simpleness was measured in two ways: by the *SI*, which compares the relative power of the simple-like (h_{1st}) and complex-like (h_{2Diag}) components of receptive field estimates (RF, middle), and by the *SI**, which measures the balance between simple-like and complex-like synaptic contributions once the stimulus-dependent receptive fields have been convolved with the corresponding stimulus sequences (RF * Stim, right). In sparse stimulation conditions, as the pixels are activated one at a time, the nonlinear contributions conveyed by the off-diagonal terms of the h_{2nd} kernel have barely any weight in the response, and the output of the h_{2Diag} filter provides an almost complete estimate of the complex-like synaptic contributions. In contrast, in the dense noise condition, as multiple pixels are activated at the same time, the dynamics of the evoked complex-like response also relies on the selectivity of the h_{2Diag} receptive field components to the spatiotemporal patterns that are presented. We thus computed the convolution of the stimulus with the full second-order kernel estimate h_{2nd} to reconstruct the complex-like synaptic contributions evoked by dense noise stimuli. (**b**) Comparison of *SI* values between sparse and dense noise conditions. Left, graph shown in **Figure 3a**. Right, comparison of *SI** values. Note that over the population the *SI** values are much more aligned along the identity line than the SI values. (**c**) Data are presented as in **b** for the comparison of the Gabor noise and dense noise conditions.

receptive field components depending on the degree of sensitivity to contrast polarity along the stimulus feature dimension for which they are selective. To assess whether the stimulus-dependent changes in receptive field simpleness could arise trivially from mapping such second-order receptive field architectures with different stimulus statistics, we simulated non-adaptive receptive field models, made up of one simple-like subunit in parallel with multiple linear filters whose outputs were squared (**Fig. 6a**). By imposing in graded ways the relative weights of the quadratic and the linear components, we synthesized a set of receptive field models that each expressed a distinct degree of complex behavior. We simulated the responses to sparse noise, Gabor noise and dense noise for each of these 'non-adaptive' receptive field models and estimated the first- and second-order kernels, using the same decomposition as in our V1 cells. The *SI* measures obtained from these receptive field models did not differ between sparse and dense noise (**Fig. 6b**) or Gabor noise and dense noise conditions (**Fig. 6c**), which indicates that the effect that we observed in our V1 cell population is unlikely to be a result of any bias of our kernel estimates by the statistical properties of the visual input itself. These non-adaptive models further illustrate that, in the absence of adaptation of the receptive field simpleness, the global synaptic responses evoked by dense stimuli are expected to express more complex-like contributions than those evoked in sparse stimulation contexts; the *SI** values computed directly from the receptive field model outputs revealed much stronger complexity in dense noise than in sparse noise (**Fig. 6b**) or Gabor noise contexts (**Fig. 6c**). Taken together, these results strongly suggest that the stimulus-dependent changes observed in V1 receptive field simpleness reflect a regulatory mechanism that compensates for the relative strength with which the stimulus recruits the simple-like and complex-like receptive field components, so as to maintain the simpleness of the visually evoked synaptic drive independent of changes in input statistics.

To get an insight into the time constants of this receptive field adaptation, we averaged across cells the synaptic responses evoked by each of these stimuli (**Supplementary Fig. 9**). This mean response component, which reflects the dynamics of the complex-like contributions averaged over the population, decayed exponentially in the first few hundred milliseconds in sparse noise (τ = 740 ms), Gabor noise (τ = 820 ms) and dense noise (τ = 750 ms) conditions. If we assume this decay is related to the adaptation of the simple/complex balance, its time constant suggests that this process is not instantaneous, but is fast enough to be still relevant regarding natural viewing condition dynamics[25].

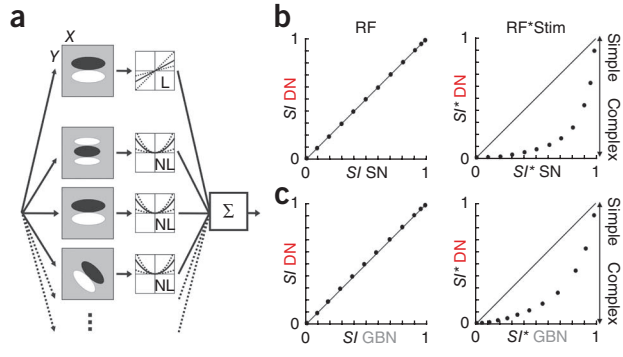

Figure 6 Simpleness in non-adaptive receptive field models. (**a**) Parallel LN cascade receptive field architecture in which linear filter outputs corresponding to different stimulus feature selectivities are passed through a second-order polynomial nonlinearity (one linear branch and several quadratic branches). In this model architecture, the linear component provides simple-like contributions, whereas the quadratic components contribute in a complex-like manner to the cell response. By keeping the same receptive field structure while imposing the relative weights of these two types of afferent components, we simulated a set of receptive fields, each expressing a fixed degree of simpleness, and simulated their responses to sparse noise, Gabor noise and dense noise stimulus sequences. (**b**) Left, comparison of the *SI* between sparse and dense noise conditions when considering the receptive fields estimated from the responses of the non-adaptive model depicted in **a**. Right, comparison of the *SI** (measured directly from the receptive field model outputs) between sparse and dense noise conditions. (**c**) Data are presented as in **b** for the comparison of the Gabor noise and dense noise conditions.

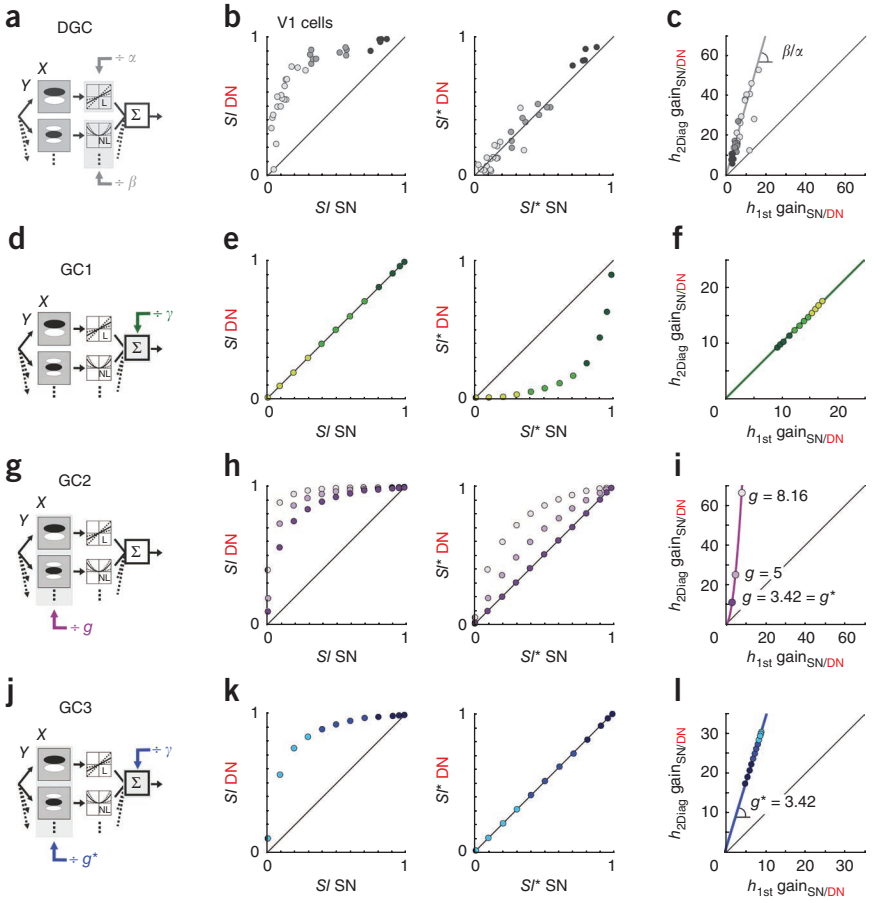

Figure 7 Simpleness in gain control receptive field models. (**a**) Differential gain control model. The adaptation of V1 receptive field simpleness can be explained by adding two separate gain control processes (α and β) to the receptive field models depicted in **Figure 6a**. These processes respectively divide simple-like and complex-like receptive field components when switching from sparse to dense noise. (**b**) Shown is the graph depicted in **Figure 5b**. (**c**) Shown is the graph depicted in **Figure 3c**. The colors of the symbols correspond to three different ranges of value for the *SI* values measured in the sparse noise condition. (**d**) Post-NL gain control model (GC1). A gain control process γ acts post-NL and normalizes the variance of the evoked response across stimulus conditions. (**e**) *SI* (left) and *SI** (right) measured from GC1 receptive field model responses in sparse and dense noise conditions. (**f**) $Gain_{SN/DN}$ measured from the h_{1st} and h_{2Diag} kernels estimated from the GC1 receptive field responses. Dark and light colors of the symbols indicate low and high values of γ, respectively. (**g**) Pre-NL gain control model (GC2). A gain control process g acts pre-NL and results in a division of linear filter outputs by g when switching from sparse noise to dense noise, independently of the receptive field simpleness. (**h**) *SI* (left) and *SI** (right) measured from GC2 receptive field model responses in sparse and dense noise conditions. (**i**) $Gain_{SN/DN}$ measured from the h_{1st} and h_{2Diag} kernels estimated from the GC2 receptive field responses. The purple curve indicates the quadratic relationship. Dark and light colors of the symbols indicate low and high values of g, respectively. g^* corresponds to the value for which we observed a complete adaptation of the receptive field simpleness between sparse noise and dense noise conditions ($SI^*_{DN} = SI^*_{SN}$). (**j**) Hybrid gain control model (GC3), a combination of the GC1 and GC2 models (with $g = g^*$). (**k**) *SI* (left) and *SI** (right) measured from GC3 model responses in sparse and dense noise conditions. (**l**) $Gain_{SN/DN}$ measured from the h_{1st} and h_{2Diag} kernels estimated from the GC3 responses. The slope of the regression line (blue) corresponds to g^*. Note that this model is mathematically equivalent to the differential gain control model (**a**) considering $\alpha = g^* \times \gamma$ and $\beta = g^{*2} \times \gamma$. Dark and light colors of the symbols indicate low and high values of γ, respectively.

Predictions by gain-control models

From the perspective of our receptive field decomposition, the most straightforward model of adaptation of V1 receptive field simpleness is to add two separate gain controls (α and β) to the receptive field models depicted in **Figure 6a**, which would account for the branch specific division of the simple-like and complex-like receptive field components, respectively, when switching from sparse to dense noise (differential gain control model; **Fig. 7a**). However, we investigated whether our results (**Fig. 7b**,**c**) could be explained by simpler adaptive models, in which the gain control process does not require any prior distinction between afferent receptive field components regarding the simple or complex nature of their contributions.

In the receptive field architecture described above (**Fig. 6a**), a minimal hypothesis for adaptation of the cell response to the stimulus strength is to assume the existence of a gain control process γ that acts after the nonlinear filtering stage (post-NL) and changes the integrative properties of the model by normalizing the variance of the evoked response with regard to the increase in the stimulus power (GC1; **Fig. 7d**). As this GC1 model affects the simple-like and complex-like afferent contributions equally, it is unable to explain any adaptation of the receptive field simpleness between sparse and dense noise (**Fig. 7e**), and the visually evoked responses remain much more complex in dense than in sparse visual conditions (**Fig. 7e**). Still, one peculiar aspect of this model is that the gain factors measured on h_{1st} and h_{2Diag} kernels are linearly related and inversely correlated with the degree of simpleness of the receptive field (**Fig. 7f**), similar to what we found experimentally (**Fig. 7c** and **Supplementary Fig. 4**).

Another minimal adaptation hypothesis is to consider a gain control process before the nonlinear filtering stage (pre-NL), that rescales the gain of the afferent subunits with regard to the increase in the stimulus power[26] (GC2; **Fig. 7g**). In this normalization model, all of the linear filtering stages are divided by a single factor, g, and the second-order receptive field components, which are related to the squared output nonlinearities, are scaled as g^2. Consequently, the receptive field simpleness is expected to increase with the visual input strength. This type of model can partially account for our results; for a given receptive field structure, one can find a particular value g^* for the divisive gain, corresponding to an under-adaptation of the linear components, but for which the increase of receptive field simpleness between sparse noise and dense noise (**Fig. 7h**) compensates exactly for the strength with which these two stimuli recruit simple-like and complex-like receptive field components (**Fig. 7h** and **Supplementary Note 2**). However, the GC2 model implies a quadratic relationship between the apparent scaling factors on simple-like and complex-like receptive field components (**Fig. 7i**), which is not consistent with our data. Moreover, in this model, different values of gain control g necessarily lead to different degrees of

adaptation of the receptive field simpleness (**Fig. 7h**). Thus, the GC2 model cannot explain both the diversity in the $gain_{SN/DN}$ values and the invariance of the SI^* across stimulus conditions.

Notably, the combination of the two mechanisms, the pre-NL gain control g^* and the post-NL gain control γ(GC3; **Fig. 7j**), appeared to be sufficient to account for both the invariance of the SI^* (**Fig. 7k**) between sparse and dense visual contexts and the linear relationship between h_{1st} and h_{2Diag} gain factors (**Fig. 7l**). This GC3 model illustrates that the adaptation of V1 receptive field simpleness can be explained by gain control processes independent of the functional distinction between simple-like and complex-like receptive field components. Nevertheless, this conclusion holds only for the parameters described above (**Fig. 7**): none of these models is suitable for explaining a differential reorganization of simple-like and complex-like spatiotemporal profiles between sparse and dense visual contexts (**Figs. 2** and **4**). More realistic network architecture and/or gain controls with additional dynamic nonlinearities are needed to explain the spatiotemporal specificity of these kernel waveform changes.

DISCUSSION

Our results show that the balance between simple-like and complex-like receptive field components depends on the statistics of the visual input, such as the same receptive field appearing to be more simple-like in dense than in sparse visual conditions. Stimulus-dependent changes in the simple or complex behavior of V1 cells have already been reported in earlier studies using drifting grating stimuli, as a function of stimulus contrast and receptive field surround recruitment[13,17,27]. However, our study is the first, to the best of our knowledge, to show such clear changes in terms of spatiotemporal reorganizations of synaptic and discharge fields at the single cell level, interpretable as a coherent adaptive behavior at the population level. This stimulus dependence of V1 receptive field simpleness does not exclude the possible existence of different classes of cells (in terms of afferent connectivity) in the cortical population. Our results instead suggest that it reflects an adaptation of the 'effective connectivity' of the network[28] to the statistical properties of the stimulus, making the balance between simple-like and complex-like synaptic influences (SI^*) afferent to any cortical cell invariant from changes in visual input statistics. If one accepts the simplified view that the SI reflects, for any given receptive field, the relative dominance of the local thalamic drive[29,30], it is likely that even in cells that receive direct geniculo-cortical afferents (in cat area 17, those in layer 4 and to a lesser extent layer 6)[31], the receptive field simpleness adaptation remains proportional to the small effect of the complex-like contributions that they might receive (as for the cells close to the point where $SI_{DN} = SI_{SN} = 1.0$; **Fig. 3a**). Our anatomical reconstruction of four cells labeled with biocytin supports the view that, whatever their rank in the thalamo-cortical layer hierarchy, all cortical cells are likely to exhibit an adaptation of their receptive field simpleness with graded extent (**Supplementary Fig. 10**). This conclusion is consistent with the previously described stimulus dependence of linear kernel estimates in superficial versus input layers[22,23]. Our data further suggest the existence of an adaptation process that would result, across all cortical layers, in a rescaling of the complex-like components in proportion with the gain control affecting the simple-like components. The effects that we describe are more detectable at the subthreshold than at the spiking level, where additional static nonlinearities may interfere with the global read-out of the connectivity rule (**Supplementary Fig. 3**).

Our results must be interpreted in a functional perspective and several non-exclusive mechanisms can still be considered. Our data do not completely exclude the contribution of a subcortical adaptation process that would make the LGN inputs to the cortex more nonlinear in sparse visual conditions than in dense visual contexts[32,33]. However, this interpretation is insufficient to account for the fact that the Gabor noise stimuli induced V1 receptive field changes that are consistent with the sparse nature of the stimulation in the orientation domain, whereas they likely correspond to dense visual inputs for retinal or thalamic cells in view of the range of spatial frequencies used[34].

Notably, our simulations indicate that a simple gain control model (**Fig. 7j**) can partially reproduce the adaptation of V1 receptive field simpleness, provided there is a specific rescaling of the strength of the inputs to the network, combined with a gain control of the amplification performed by the downstream cell. Literally, the model suggests that this adaptive behavior could result from a combination of activity-dependent adaptation at the thalamic level, synaptic depression at thalamo-cortical synapses or any mechanism that reduces the effect of the feed-forward drive, and synaptic depression at cortico-cortical synapses, increased levels of intracortical inhibition, activity-dependent changes in cell intrinsic properties or any mechanism that reduces the intracortical amplification.

The increase of receptive field simpleness in dense visual conditions could also be explained by a change in the balance between excitation and inhibition[35] resulting in a suppression of the complex-like synaptic components estimated in the sparse noise context. In a generalized feed-forward perspective, this suppression could either come from an increase of push-pull inhibition[36] or from the enhancement of an unselective complex inhibition[37–39] (**Supplementary Fig. 11**), but in both cases, the apparent increase of receptive field linearity in the dense noise condition would result from the interaction between excitatory and inhibitory nonlinear inputs.

Another interpretation would be to consider the idea that the simple or complex nature of V1 receptive fields arises from a variable balance between feed-forward and lateral inputs[10,11,40], the feed-forward drive providing the simple-like component while the recurrent lateral connections convey complex-like contributions. Accordingly, our results might be explained by the functional recruitment of lateral interactions in sparse stimulation conditions and by the decoupling of adjacent cortical columns in dense visual contexts (**Supplementary Fig. 11**). This view is supported by recent results suggesting that the lateral propagation of activity between adjacent cortical units decreases substantially when the stimulus contrast is increased[41]. In view of our own results, the stimulus dependence of the lateral cortical interactions likely generalizes to other stimulus dimensions, rather than remain exclusive to the local contrast. Similar effects might be obtained by increasing the spatial or temporal density of the stimulus, with the important parameter probably being the effective contrast along the stimulus feature dimensions for which the cell is selective[42,43].

Regardless of the mechanisms underlying this adaptive behavior, one last question is the relevance of this adaptation in natural viewing conditions. The synaptic normalization process that we found could maintain in V1 the relative contribution of linear and nonlinear synaptic inputs invariant to dynamic changes in the local spatiotemporal context of the visual scene. During oculomotor exploration, depending on eye fixation location, a given receptive field would sample locally sparser or denser regions of a natural scene; synaptic normalization would allow the activated network to extract the same relative amount of information along the phase-sensitive and the phase-insensitive processing streams, thus ensuring the detection of the most relevant features of the visual scene independently of the local context in which they are embedded. This would improve

information transmission by avoiding the over-representation of second-order correlations among cell population responses in dense visual contexts while increasing their detectability in sparse contexts, thus adapting the neuron's dynamic range to the level of correlation present in the visual input. We propose that the stimulus dependence of V1 receptive field simpleness reflects a general rule of functional homeostasis common to many sensory systems[33,44–47], which would ensure the adaptation of the network nonlinearities to ongoing changes in the statistical structure of the sensory input, according to optimal encoding principles[48].

METHODS

Methods and any associated references are available in the online version of the paper at http://www.nature.com/natureneuroscience/.

Note: Supplementary information is available on the Nature Neuroscience website.

ACKNOWLEDGMENTS

We are thankful to G. Sadoc for his invaluable technical assistance in developing the stimulation software and kernel analysis library tools. We thank A. Davison for comments and suggestions on the manuscript. We are thankful to Z. Kisvarday and K. Sari for their help in the biocytin labeling protocol. We acknowledge the financial support of CNRS, the Agence Nationale de la Recherche (Natstats and V1-Complex), European community contracts Facets (FP6-2004-IST-FETPI 15879) and Brain-i-nets (FP7-2009-ICT-FET 243914).

AUTHOR CONTRIBUTIONS

The study was conceived by J.F., C.M. and Y.F. The experiments were performed by J.F., C.M. and M.P. J.F. performed the data analysis and model simulations. J.F., C.M. and Y.F. wrote the paper.

COMPETING FINANCIAL INTERESTS

The authors declare no competing financial interests.

Published online at http://www.nature.com/natureneuroscience/.
Reprints and permissions information is available online at http://www.nature.com/reprints/index.html.

1. Hubel, D.H. & Wiesel, T. Receptive fields, binocular interaction and functional architecture in the cat's visual cortex. *J. Physiol. (Lond.)* **160**, 106–154 (1962).
2. Movshon, J.A., Thompson, I. & Tolhurst, D. Spatial summation in the receptive fields of simple cells in the cat's striate cortex. *J. Physiol. (Lond.)* **283**, 53–77 (1978).
3. DeAngelis, G.C., Ohzawa, I. & Freeman, R.D. Spatiotemporal organization of simple-cell receptive fields in the cat's striate cortex. II. Linearity of temporal and spatial summation. *J. Neurophysiol.* **69**, 1118–1135 (1993).
4. Carandini, M. *et al.* Do we know what the early visual system does? *J. Neurosci.* **25**, 10577–10597 (2005).
5. Movshon, J.A., Thompson, I. & Tolhurst, D. Receptive field organization of complex cells in the cat's striate cortex. *J. Physiol. (Lond.)* **283**, 79–99 (1978).
6. Dean, A.F. & Tolhurst, D.J. On the distinctness of simple and complex cells in the visual cortex of the cat. *J. Physiol. (Lond.)* **344**, 305–325 (1983).
7. Emerson, R.C. *et al.* Nonlinear directionally selective subunits in complex cells of cat striate cortex. *J. Neurophysiol.* **58**, 33–65 (1987).
8. Skottun, B.C. *et al.* Classifying simple and complex cells on the basis of response modulation. *Vision Res.* **31**, 1079–1086 (1991).
9. Priebe, N.J. *et al.* The contribution of spike threshold to the dichotomy of cortical simple and complex cells. *Nat. Neurosci.* **7**, 1113–1122 (2004).
10. Chance, F.S., Nelson, S.B. & Abbott, L.F. Complex cells as cortically amplified simple cells. *Nat. Neurosci.* **2**, 277–282 (1999).
11. Tao, L. *et al.* An egalitarian network model for the emergence of simple and complex cells in visual cortex. *Proc. Natl. Acad. Sci. USA* **101**, 366–371 (2004).
12. Rust, N.C. *et al.* Spatiotemporal elements of macaque v1 receptive fields. *Neuron* **46**, 945–956 (2005).
13. Bardy, C. *et al.* "Simplification" of responses of complex cells in cat striate cortex: suppressive surrounds and "feedback" inactivation. *J. Physiol. (Lond.)* **574**, 731–750 (2006).
14. Victor, J.D. *et al.* Responses of V1 neurons to two-dimensional hermite functions. *J. Neurophysiol.* **95**, 379–400 (2006).
15. Albrecht, D.G., Farrar, S.B. & Hamilton, D.B. Spatial contrast adaptation characteristics of neurones recorded in the cat's visual cortex. *J. Physiol. (Lond.)* **347**, 713–739 (1984).
16. Ohzawa, I., Sclar, G. & Freeman, R.D. Contrast gain control in the cat's visual system. *J. Neurophysiol.* **54**, 651–667 (1985).
17. Carandini, M. & Ferster, D. A tonic hyperpolarization underlying contrast adaptation in cat visual cortex. *Science* **276**, 949–952 (1997).
18. Sanchez-Vives, M.V., Nowak, L.G. & McCormick, D.A. Membrane mechanisms underlying contrast adaptation in cat area 17 *in vivo*. *J. Neurosci.* **20**, 4267–4285 (2000).
19. Sharpee, T.O. *et al.* Adaptive filtering enhances information transmission in visual cortex. *Nature* **439**, 936–942 (2006).
20. Felsen, G. *et al.* Cortical sensitivity to visual features in natural scenes. *PLoS Biol.* **3**, e342 (2005).
21. David, S.V., Vinje, W.E. & Gallant, J.L. Natural stimulus statistics alter the receptive field structure of v1 neurons. *J. Neurosci.* **24**, 6991–7006 (2004).
22. Yeh, C.I. *et al.* Stimulus ensemble and cortical layer determine V1 spatial receptive fields. *Proc. Natl. Acad. Sci. USA* **106**, 14652–14657 (2009).
23. Victor, J.D. *et al.* Laminar and orientation-dependent characteristics of spatial nonlinearities: implications for the computational architecture of visual cortex. *J. Neurophysiol.* **102**, 3414–3432 (2009).
24. Mata, M.L. & Ringach, D.L. Spatial overlap of ON and OFF subregions and its relation to response modulation ratio in macaque primary visual. *J. Neurophysiol.* **93**, 919–928 (2005).
25. Stryker, M. & Blakemore, C. Saccadic and disjunctive eye movements in cats. *Vision Res.* **12**, 2005–2013 (1972).
26. Carandini, M. & Heeger, D.J. Summation and division by neurons in primate visual cortex. *Science* **264**, 1333–1336 (1994).
27. Crowder, N.A. *et al.* Complex cells increase their phase sensitivity at low contrasts and following adaptation. *J. Neurophysiol.* **98**, 1155–1166 (2007).
28. Aertsen, A.M. *et al.* Dynamics of neuronal firing correlation: modulation of "effective connectivity". *J. Neurophysiol.* **61**, 900–917 (1989).
29. Martinez, L.M. & Alonso, J.M. Construction of complex receptive fields in cat primary visual cortex. *Neuron* **32**, 515–525 (2001).
30. Martinez, L.M. *et al.* Receptive field structure varies with layer in the primary visual cortex. *Nat. Neurosci.* **8**, 372–379 (2005).
31. LeVay, S. & Gilbert, C.D. Laminar patterns of geniculocortical projection in the cat. *Brain Res.* **113**, 1–19 (1976).
32. Lesica, N.A. *et al.* Adaptation to stimulus contrast and correlations during natural visual stimulation. *Neuron* **55**, 479–491 (2007).
33. Smirnakis, S.M. *et al.* Adaptation of retinal processing to image contrast and spatial scale. *Nature* **386**, 69–73 (1997).
34. So, Y.T. & Shapley, R. Spatial tuning of cells in and around lateral geniculate nucleus of the cat: X and Y relay cells and perigeniculate interneurons. *J. Neurophysiol.* **45**, 107–120 (1981).
35. Sillito, A.M. The contribution of inhibitory mechanisms to the receptive field properties of neurones in the striate cortex of the cat. *J. Physiol. (Lond.)* **250**, 305–329 (1975).
36. Troyer, T.W. *et al.* Contrast-invariant orientation tuning in cat visual cortex: thalamocortical input tuning and correlation-based intracortical connectivity. *J. Neurosci.* **18**, 5908–5927 (1998).
37. Lauritzen, T.Z. & Miller, K.D. Different roles for simple-cell and complex-cell inhibition in V1. *J. Neurosci.* **23**, 10201–10213 (2003).
38. Hirsch, J.A. *et al.* Functionally distinct inhibitory neurons at the first stage of visual cortical processing. *Nat. Neurosci.* **6**, 1300–1308 (2003).
39. Liu, B.H. *et al.* Visual receptive field structure of cortical inhibitory neurons revealed by two-photon imaging guided recording. *J. Neurosci.* **29**, 10520–10532 (2009).
40. Debanne, D., Shulz, D.E. & Fregnac, Y. Activity-dependent regulation of "on" and "off" responses in cat visual cortical receptive fields. *J. Physiol. (Lond.)* **508**, 523–548 (1998).
41. Nauhaus, I. *et al.* Stimulus contrast modulates functional connectivity in visual cortex. *Nat. Neurosci.* **12**, 70–76 (2009).
42. Müller, J.R. *et al.* Rapid adaptation in visual cortex to the structure of images. *Science* **285**, 1405–1408 (1999).
43. Felsen, G. *et al.* Dynamic modification of cortical orientation tuning mediated by recurrent connections. *Neuron* **36**, 945–954 (2002).
44. Nagel, K.I. & Doupe, A.J. Temporal processing and adaptation in the songbird auditory forebrain. *Neuron* **51**, 845–859 (2006).
45. Maravall, M. *et al.* Shifts in coding properties and maintenance of information transmission during adaptation in barrel cortex. *PLoS Biol.* **5**, e19 (2007).
46. Higley, M.J. & Contreras, D. Frequency adaptation modulates spatial integration of sensory responses in the rat whisker system. *J. Neurophysiol.* **97**, 3819–3824 (2007).
47. Brenner, N., Bialek, W. & de Ruyter van Steveninck, R. Adaptive rescaling maximizes information transmission. *Neuron* **26**, 695–702 (2000).
48. Wainwright, M.J. Visual adaptation as optimal information transmission. *Vision Res.* **39**, 3960–3974 (1999).

ONLINE METHODS

Animal preparation and electrophysiological recordings. Data presented here were obtained from anesthetized (alfatesin) and paralyzed cats, according to the American Physiological Society's Guiding Principles for the Care and Use of Animals. The animals used in these experiments were bred in the Central CNRS Animal Care (French Agriculture Ministry Authorization: B91-272-105) under required veterinary and National Ethical Committee supervision. Intracellular electrodes were made from 1.5-mm-thick borosilicate pipettes filled with a solution of 2 M potassium methyl sulfate and 4 mM KCl. In some experiments, we labeled intracellularly the cells that we recorded by adding 1% biocytin (wt/vol) to the intra-pipette solution. Electrode resistances ranged from 60 to 90 MΩ. Recordings were performed using an Axoclamp 2A amplifier.

Visual stimulation. Visual stimuli were generated using in-house software (Elphy, G. Sadoc, UNIC-CNRS) and presented on a gamma-corrected monitor with a refresh rate of 150 Hz and a background luminance of 12 cd m^{-2}. Three kinds of white noise stimuli were presented in the same explored visual area: two-dimensional ternary sparse noise (random sequences of non-overlapping white (23 cd m^{-2}) or black (1 cd m^{-2}) squares, presented one at a time on a uniform luminance background (12 cd m^{-2}) over a 10 × 10 grid (except for cell 2, 15 × 15)), two-dimensional ternary dense noise (random sequences of squares (same squares as in the corresponding sparse noise condition), which could be either white (23 cd m^{-2}), black (1 cd m^{-2}) or equal to the background (12 cd m^{-2}) with equal probability), and Gabor noise (consisting of random sequences of flashed Gabor stimuli). Michelson's contrast was held constant at 0.5 and the spatial Gabor attenuation constant was 40% of the explored region dimensions. For each frame, orientation, spatial frequency and spatial phase were randomly chosen from a discrete uniform distribution consisting of six orientations ranging from 0° to 150°, five spatial frequencies ranging from 0.2 to 1.1 cycles per degree, and four spatial phases ranging from 0 to 270°.

The seed used for initializing the random process of these three white noise stimuli was changed for each sequence (a necessary condition in sparse sequences to estimate the receptive field function). For each cell, visual stimuli were presented in an interleaved way, in the same region of the visual field and at the same frequency (frame duration: 13 ms for 15 cells, 26 ms for 12 cells, 33 ms for 4 cells and 56 ms for 1 cell). We adapted the size of the explored visual area to the apparent spatial extent of the receptive field. Still, the number of pixels covering the significant receptive field area (sparse noise and dense noise conditions) varied from cell to cell (from 4 to 54 pixels) and was, on average, 20 pixels.

Note that although sparse and dense noise stimuli exhibited the same elementary contrast steps (c), they differed strongly in spatiotemporal statistics. In the sparse noise condition, as pixels are activated only one at a time, the power of the stimulus (P^2) is very low ($P^2 = \frac{2}{200} \times c^2$ for a 10 × 10 simulation grid). This is in contrast with the dense noise condition, where the three luminance states are, on average, equally represented in each frame ($P^2 = \frac{2}{3}c^2$). These differences between sparse and dense stimulation regimes give a ratio between their respective s.d. of luminance values of $\sqrt{\frac{2/3}{2/200}} \approx 8.16$.

Second-order Volterra kernel estimation. Action potentials, when present, were automatically filtered out from synaptic fluctuations offline. First- and second-order receptive field components were estimated using a least-squares method, considering either the spiking response or the subthreshold fluctuations. This estimation consisted of solving the system of equations corresponding to the Volterra series expansion

$$R(t) = h_0 + \sum_{x,y,\tau} h_{1st}(x,y,\tau) \times S(x,y,t-\tau) + \sum_{x_1,y_1,\tau_1} \sum_{x_2,y_2,\tau_2} h_{2nd}(x_1,y_1,\tau_1,x_2,y_2,\tau_2) \times S(x_1,y_1,t-\tau_1) \times S(x_2,y_2,t-\tau_2) \quad (1)$$

where $R(t)$ is the cell response recorded at time t, sampled with a 1-ms resolution, S is the stimulus input vector (see **Supplementary Note 3**), and h_0, h_{1st}, h_{2nd} correspond to the zero- , first- and second-order Volterra kernels, respectively.

The kernels estimated from responses to Gabor noise obeyed the same formalism as in the spatiotemporal domain except that h_{1st} and h_{2nd} were functions of position in the Fourier space. In this condition, contrast of opposite signs corresponded to identical Gabor stimuli, but with spatial phases separated by 180°.

Note that, as a result of the sparse statistical structure of sparse noise and Gabor noise stimuli, the off-diagonal elements of the h_{2nd} kernel are barely stimulated, which means that the estimation of the second-order receptive field components comes down to the estimation of its diagonal elements h_{2Diag} ($h_{2Diag}(x,y,\tau) = h_{2nd}(x,y,\tau,x,y,\tau)$). Consequently, in these sparse stimulation conditions, the second-order Volterra decomposition (equation (1)) can be simplified as

$$R(t) = h_0 + \sum_{x,y,\tau} h_{1st}(x,y,\tau) \times S(x,y,t-\tau) + \sum_{x,y,\tau} h_{2Diag}(x,y,\tau) \times S(x,y,t-\tau)^2 \quad (2)$$

In contrast, in the dense noise condition, the full second-order kernel (diagonal and off-diagonal elements) is stimulated such that it is possible to estimate it completely. Still, as a result of the high dimensionality of this functional space, the estimation of the off-diagonal elements is constrained by the recording length. Although the number of collected spikes was generally too small to compute this estimate, our voltage records allowed us to proceed to the estimation of the off-diagonal elements of the second-order kernel for all cells. To keep a ratio of at least 1:5 between the number of kernel parameters and the number of data points, we had to restrict spatially and temporally the estimation of these off-diagonal terms. Nonetheless, despite this constraint, we were able, for all cells, to cover in the off-diagonal space the elements corresponding to the full spatiotemporal extent of the significant responses estimated in the h_{2Diag} component. Note that the estimation of the h_{2Diag} kernel parameters was unchanged whether we considered the estimation of the off-diagonal elements of the second-order kernel or not.

Variance of kernel estimates. The statistical significance of kernel parameters was computed as spatiotemporal z-score maps in which each kernel parameter (corresponding to a particular spatiotemporal position) was divided by the s.d. of the kernel error calculated from the parameter covariance matrix. A major benefit of using least-squares methods is that it provides a direct theoretical expression of the confidence bounds to take into consideration for kernel parameters[49]. If we assume that the corrupting noise in the output is a stimulus-independent Gaussian process with zero-mean and variance σ^2, the variance of each kernel parameter is given by the corresponding elements on the diagonal of the parameter covariance matrix C_θ, which is computed from the inverse of the stimulus covariance matrix **H** (Hessian matrix) and an unbiased estimate of the residual variance σ^2_{res},

$$C_\theta = \sigma^2_{res} \times H^{-1} \quad (3)$$

where

$$\sigma^2_{res} = \frac{1}{N-M} \times \sum_t (R(t) - \hat{R}(t))^2 \quad (4)$$

with N being the number of time bins, M being the number of kernel parameters and $\hat{R}(t)$ being the response output reconstructed from the estimated kernels.

Variance of the kernels output. As the kernel outputs are linearly related to their parameters, the variance of the error of the convolution product at time t between the stimulus sequence and the kernel ($(h_{1st} \times S)_t$ or $(h_{2nd} \times S)_t$) can be deduced from the parameter covariance matrix C_θ[49]

$$\sigma^2_{(h^*S)(t)} = U_h(t)^T \times C_\theta \times U_h(t) \quad (5)$$

where $U_h(t)$ is a vector which contains the appropriate stimulus elements (that is, $S(x,y,t-\tau)$ or $S(x_1,y_1,t-\tau_1) \times S(x_2,y_2,t-\tau_2)$) in positions corresponding to the parameters of the considered kernel and is zero elsewhere.

Quantification of kernel estimates. All kernel quantifications were based on the total duration of the impulse responses instead of selecting one particular time epoch (such as when the receptive field amplitude or spatial extent is maximal). To avoid any contamination of our measurements by the residual noise of our

kernel estimates, we only considered spatiotemporal positions that were statistically significant (z score ≥ 2.33, $P \leq 0.01$). The SI was defined as

$$SI = \frac{\sum_{x,y,\tau} h_{1st}(x,y,\tau)^2}{\sum_{x,y,\tau} h_{1st}(x,y,\tau)^2 + \sum_{x,y,\tau} h_{2Diag}(x,y,\tau)^2} \quad (6)$$

The relationship between dense noise and sparse noise SI values (**Fig. 3a** and **b**) was fitted by

$$SI_{DN} = \frac{SI_{SN}}{SI_{SN} + \left(\frac{1}{k}\right)^2 \times (1 - SI_{SN})} \quad (7)$$

where k is a constant parameter over the cell population (see **Supplementary Note 1**).

The gain factor $\text{gain}_{\text{sparse/dense}}$ between sparse noise and dense noise kernels was defined as the ratio of the kernel Euclidian norms associated with the different stimulus conditions, considering the kernels as spatiotemporal vectors

$$h\,\text{gain}_{SN/DN} = \frac{\sqrt{\sum_{x,y,\tau} h^{SN}(x,y,\tau)^2}}{\sqrt{\sum_{x,y,\tau} h^{DN}(x,y,\tau)^2}} \quad (8)$$

SI^*, which measures the strength of the simple-like and complex-like components of the synaptic response, was computed from the convolution products between the visual stimulus and the first-order (h_{1st}) or second-order (h_{2nd}) kernels, considering only the components of the kernel output that were statistically significant (z score ≥ 2.33, $P \leq 0.01$).

$$SI^* = \frac{\sum_t (h_{1st} \bullet S_t)^2}{\sum_t (h_{1st} \bullet S_t)^2 + \sum_t (h_{2nd} \bullet S_t)^2} \quad (9)$$

where the • symbol denotes the convolution product between the first- or second-order kernel and the stimulus sequence (see equation (1)).

Note that, in sparse noise and Gabor noise conditions, given that the h_{2nd} kernel comes down to its diagonal elements h_{2Diag}, the expression of SI^* is equivalent to

$$SI^* = \frac{\sum_t (h_{1st} \bullet S_t)^2}{\sum_t (h_{1st} \bullet S_t)^2 + \sum_t (h_{2Diag} \bullet S_t)^2} \quad (10)$$

Areas delimited by contours of 99% significant responses (z score ≥ 2.33, $P \leq 0.01$) were measured for each kernel on spatially smoothed versions of their respective z-score maps and plotted over time. The maximal spatial extent of these contours (measured by their equivalent apparent diameter expressed in degrees of visual angle) as well as the timing of this maximum (peak latency) was measured for each kernel to be compared between conditions. The onset latency of each kernel was derived from the contour area measurement. The initial radial growth of the significant responsive area was generally constant as a function of time and we computed the onset time by defining an area threshold corresponding to half of the maximum and then moving backwards in time until the time derivative of the receptive field area fell below 10% of the derivative calculated at half-amplitude, for five continuous time steps (5 ms). This measure thus reflects the latency of the earliest response, which initiates the progressive build-up of the full receptive field domain. We found much more reliable measurements using this method than with methods based on the derivative of the kernel waveforms.

Predictive power of receptive field estimates. We assessed the ability of sparse noise and dense noise receptive field estimates to predict responses to new datasets which were not used for estimating the kernels. Receptive field estimates were first convolved with the validation stimulus sequence according to equation (1) and rescaled according to the best linear coefficient (in the least-squares sense) to avoid any failure of prediction just due to a static change in the linear gain. Predicted and recorded responses were low-pass filtered at 75 Hz and binned at 1-ms resolution. We quantified the accuracy of the prediction by measuring the predictive power, defined as the percentage of variance of the cell response explained by the prediction, and the predictive correlation, defined as the Pearson's correlation coefficient between measured and predicted responses.

$$\text{Predictive power} = 100 \times \left(1 - \frac{\sum (V_m(t) - \hat{V}_m(t))^2}{\sum (V_m(t) - \langle V_m \rangle)^2}\right) \quad (11)$$

$$\text{Predictive correlation} = \frac{\sum (V_m(t) - \langle V_m \rangle) \times (\hat{V}_m(t) - \langle \hat{V}_m \rangle)}{\sqrt{\sum (V_m(t) - \langle V_m \rangle)^2 \times \sum (\hat{V}_m(t) - \langle \hat{V}_m \rangle)^2}} \quad (12)$$

where $\hat{V}_m$ denotes the response predicted by the receptive field estimates, V_m is the recorded cell response and $\langle V_m \rangle$, the mean response level.

To predict the response to the same stimulus condition as the one used for estimating the receptive field, we considered 95% of the total recording length for kernel estimation, computed the prediction on the 5% left with the estimated kernels and repeated this procedure until we completed the prediction of the full response.

Note that, to have the longest recording duration for estimating the second-order kernels, we only recorded single trial responses (the seed of the white noise was changed every trial). Thus, given that the actual response variance also contains a certain amount of noise (which would have been reduced by averaging, had we used the same seed for all trials), our measurements of predictive power correspond to an underestimate of the true ability of receptive field estimates to predict the stimulus locked response of the validation dataset.

Receptive field simulations. Simulated receptive fields were made up of a parallel bank of linear filters (**Fig. 6a**), shaped as a sum of two or three non-overlapping Gaussian zones with alternating polarities, so that they looked like typical simple cell receptive fields. Each filter was then convolved with sparse noise, Gabor noise or dense noise sequences and their outputs were passed through a multidimensional second-order polynomial in which one of the filter outputs was linearly transformed while the others were squared. In this static nonlinearity, the strength of the first-order coefficient relative to that of the quadratic components thus influenced the simple or complex nature of the full receptive field model. This allowed us to define, in a graded way, several receptive field models with properties intermediate between purely complex and purely simple behaviors and whose degree of linearity remained the same across stimulus conditions. In addition to these non-adaptive receptive field models, we also simulated adaptive filter banks which were strictly identical to those simulated in **Figure 6**, but included gain control processes (**Fig. 7d,g,j**). In the GC1 receptive field models, the variance of the global response evoked by the stimulus sequence was forced to stay constant across stimulus conditions, by scaling the filter bank output after the nonlinear filtering stage with the appropriate factor γ. In the GC2 receptive field models, the gain of all linear subunits was divided by a constant factor g when switching from sparse noise to dense noise, regardless of the degree of linearity of the receptive field. Three different values of g were tested: $g = 8.16$, corresponding to a full adaptation of the linear outputs to the change in stimulus energy, $g = 5$, and $g = g^* = 3.42$, corresponding to a full adaptation of the simpleness of the receptive field model output between sparse noise and dense noise ($SI^*_{DN} = SI^*_{SN}$). Finally, in the GC3 receptive field models, we combined the division of the linear subunits by a factor corresponding to a complete adaptation of the SI^* ($g = g^*$) and the normalization of the variance of the filter bank output across stimulus conditions.

49. Westwick, D.T. & Kearney, R.E. *Identification of Nonlinear Physiological Systems* (Wiley-IEEE, 2003).

doi:10.1038/nn.2861